Structural basis for RNA-duplex unwinding by the DEAD-box helicase DbpA

JAN PHILIP WURM

Institute of Biophysics and Physical Biochemistry, Regensburg Center for Biochemistry, University of Regensburg, 93053 Regensburg, Germany

ABSTRACT

DEAD-box RNA helicases are implicated in most aspects of RNA biology, where these enzymes unwind short RNA duplexes in an ATP-dependent manner. During the central step of the unwinding cycle, the two domains of the helicase core form a distinct closed conformation that destabilizes the RNA duplex, which ultimately leads to duplex melting. Despite the importance of this step for the unwinding process no high-resolution structures of this state are available. Here, I used nuclear magnetic resonance spectroscopy and X-ray crystallography to determine structures of the DEAD-box helicase DbpA in the closed conformation, complexed with substrate duplexes and single-stranded unwinding product. These structures reveal that DbpA initiates duplex unwinding by interacting with up to three base-paired nucleotides and a 5′ single-stranded RNA duplex overhang. These high-resolution snapshots, together with biochemical assays, rationalize the destabilization of the RNA duplex and are integrated into a conclusive model of the unwinding process.

Keywords: DEAD-box helicase; ribosome biogenesis; molecular mechanism; RNA; NMR spectroscopy

INTRODUCTION

RNA molecules are involved in numerous cellular processes and their correct folding is often critical for function. RNA helicases that act as RNA chaperones resolve misfolded RNA structures and rearrange RNA–protein complexes consequently being essential for cellular survival (Jarmoskaite and Russell 2014).

The largest family of RNA helicases in eukaryotes is represented by DEAD-box proteins (Fairman-Williams et al. 2010). These enzymes unwind short RNA duplexes (up to 12–16 base pairs) in a nonprocessive and ATP-dependent manner. The functional core of DEAD-box helicases consists of two RecA-like domains (termed RecA_N and RecA_C for the N- and C-terminal domains, respectively). The two domains are connected by a short, flexible linker and undergo large conformational changes during the unwinding cycle (Fig. 1A; Linder and Jankowsky 2011; Putnam and Jankowsky 2013). In the apo-state, the helicase core adopts an open conformation, where the two RecA domains tumble independently (Theissen et al. 2008; Sun et al. 2014; Wurm 2020) and where ATP can bind to the RecA_N domain (Mallam et al. 2012; Samatanga and Klostermeier 2014). Binding of substrate RNA—in addition to ATP—induces the formation of a distinct closed conformation (Theissen et al. 2008; Sun et al. 2014), where ATP is sandwiched between the two domains and one of the RNA strands is bound to a bipartite active site, formed by both core domains (Sengoku et al. 2006). RNA binding to the active site leads to the destabilization of the RNA duplex and spontaneous dissociation of the unbound RNA strand (Rogers et al. 1999; Yang et al. 2007). The ATPase activity of DEAD-box helicases is greatly increased in the closed conformation. Upon ATP hydrolysis the helicase core returns to the open conformation (Theissen et al. 2008), while ADP and the single-stranded RNA (ssRNA) product dissociate due to the dissolution of the active site. ATP binding is therefore sufficient for unwinding, with ATP hydrolysis mainly serving to release the helicase from unwound ssRNA (Liu et al. 2008). In addition to the productive unwinding cycle described above, DEAD-box helicases are prone to futile cycles, which occur when ATP is hydrolyzed prior to dissociation of the RNA duplex (Fig. 1A). These futile cycles increase sharply for longer, more stable duplexes due to decreased duplex dissociation rates (Putnam and Jankowsky 2013). In addition to RNA unwinding, DEAD-box helicases can also remodel RNA/protein complexes or act as RNA-clamps (Putnam and Jankowsky 2013).

Several structures of DEAD-box helicases in the closed state, bound to ssRNA and nonhydrolyzable ATP analogs

Corresponding author: jan-philip.wurm@ur.de

Article is online at http://www.rnajournal.org/cgi/doi/10.1261/rna.079582.123. Freely available online through the *RNA* Open Access option.

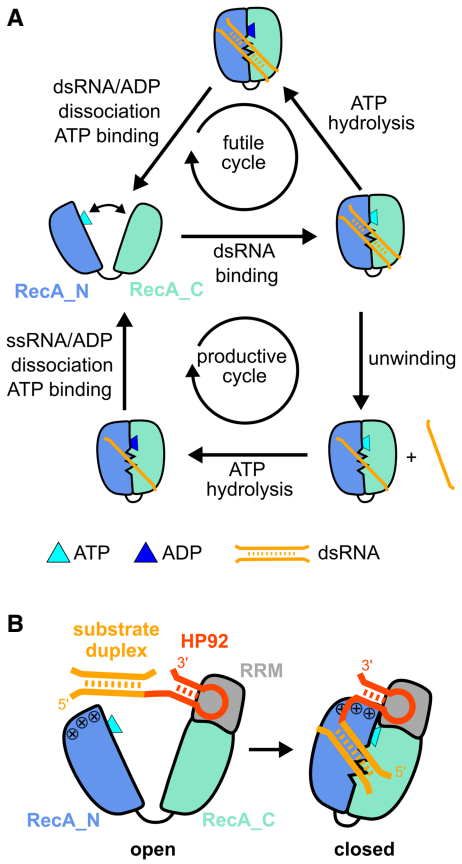

FIGURE 1. Unwinding cycle of DEAD-box helicases and activation of DbpA by HP92 RNA. (*A*) Schematic diagram of futile cycles (*top*) and productive unwinding cycles (*bottom*) of DEAD-box helicases. The helicase core (RecA_N domain blue, RecA_C domain cyan) alternates between an open conformation in the apo or ATP-bound state and a closed conformation in the presence of ATP and RNA. (*B*) Domain orientation of DbpA in the open (*left*) and closed state (*right*). The C-terminal RNA recognition motif (RRM) (gray) orients HP92 (red) such that the stem of HP92 forms favorable interactions with a positively charged patch (indicated by + signs) on the RecA_N domain in the closed state. This stabilizes the closed state and enables the recruitment of the substrate duplex (orange, located 5′ to HP92) to the active site of the helicase core.

were determined in the last 15 years (Sengoku et al. 2006; Collins et al. 2009; Del Campo and Lambowitz 2009; Montpetit et al. 2011; Wong et al. 2016; Ren et al. 2017; Ngo et al. 2019; Chen et al. 2020). Consequently, such structures correspond to the product-bound state following duplex unwinding and prior to ATP hydrolysis. The structures revealed a conserved ssRNA binding mode (Supplemental Fig. S1), where the bipartite, active site of the helicase core interacts with the sugar and phosphate backbone of six single-stranded nucleotides (nt). The RNA adopts a bent conformation due to the interaction between the RNA backbone and several highly conserved sequence motifs within the helicase core domains. This RNA conformation strongly differs from the canonical A-form helical conformation and is thus incompatible with duplex formation (Russell et al. 2013). In agreement with the sequence-independent unwinding activity of DEAD-box helicases, no interactions are formed between the active site and RNA bases. In contrast to this wealth of structural information for the product-bound state, a structure of the closed conformation complexed with double-stranded RNA (dsRNA) substrate and ATP analog is still missing. It is therefore unclear how the central step of the unwinding process—namely, the destabilization of the RNA duplex—is achieved at the molecular level.

A major challenge in the structural characterization of the destabilized duplex state lies in the trapping of this inherently unstable state in a homogeneous conformation. This is further complicated by the lack of sequence-specificity that facilitates binding in differing registers to the RNA. In order to overcome these challenges, I selected the *Escherichia coli* DEAD-box helicase DbpA for structural studies. DbpA possesses a C-terminal RNA recognition motif (RRM) (Wang et al. 2006) in addition to the helicase core and we recently demonstrated that this RRM domain is stably anchored to the RecA_C domain (Fig. 1B; Wurm et al. 2021). DbpA is involved in ribosome maturation (Sharpe Elles et al. 2009) and is recruited to the nascent ribosome by a specific, high-affinity interaction between the RRM and hairpin 92 (HP92) of the 23S rRNA (Fig. 1B; Diges and Uhlenbeck 2001; Hardin et al. 2010). Binding of HP92 is necessary for the helicase activity of DbpA, as a direct interaction between RRM-bound HP92 and the RecA_N domain strongly stabilizes—and thereby enables—formation of the closed conformation (Wurm et al. 2021). A substrate duplex linked to HP92 is therefore recruited to DbpA with high affinity and can also be efficiently unwound. Meanwhile, attachment onto HP92 locks the substrate duplex in a well-defined position relative to the active site of the helicase core and consequently stabilizes the helicase/substrate complex. Interestingly, attachment of the substrate duplex to HP92 is not necessary for unwinding by DbpA and HP92 also supports unwinding when added in-trans together with a substrate duplex lacking HP92.

In this study, I used nuclear magnetic resonance (NMR) spectroscopy to identify suitable ATP analogs and RNA constructs that enable trapping of DbpA in complex with a destabilized duplex. Based on these results crystal structures of DbpA in its closed state were solved. These structures show how the active site of the helicase core interacts with two different substrate RNAs: an RNA hairpin loop and a ss/dsRNA junction. In addition, the structure of DbpA in complex with ssRNA product was determined. These structures can be readily integrated into a model of the unwinding cycle, where interactions between helicase and the ss/dsRNA junction rationalize how DbpA achieves the RNA duplex destabilization and promotes unwinding.

RESULTS

A hairpin RNA substrate in combination with ADP/BeF_3 traps the destabilized duplex state

In order to gain insights into the molecular mechanism that underlies duplex destabilization by DbpA during unwinding, I set out to identify conditions that trap the helicase when complexed with an unwinding intermediate. Since ATP binding is sufficient for unwinding, with ATP hydrolysis solely required for helicase recycling (Liu et al. 2008), I screened for suitable nonhydrolyzable ATP analogs that support the formation of the closed state, based on their ability to fuel duplex unwinding by DbpA during single-turnover unwinding assays. To allow for unwinding by DbpA, the RNA construct included HP92 together with the substrate duplex consisting of 9 bp (Fig. 2A). From the four investigated ATP analogs (ADPNP, ADPCP, ATPγS, and ADP/BeF_3), only ATPγS (k_{obs} 0.04 ± 0.01 min^{-1}) and ADP/BeF_3 (k_{obs} 0.10 ± 0.01 min^{-1}) supported unwinding of the RNA substrate on a similar timescale as ATP (k_{obs} 0.43 ± 0.02 min^{-1}). Interestingly, ATPγS was hydrolyzed during the unwinding process (Supplemental Fig. S2) and is therefore not suitable for trapping the destabilized duplex over extended periods. Based on these results, ADP/BeF_3 was used for further investigations.

To enforce trapping of the destabilized duplex by DbpA and to prevent the dissociation of the RNA duplex, an RNA construct (hp-HP92 RNA) containing a hairpin structure

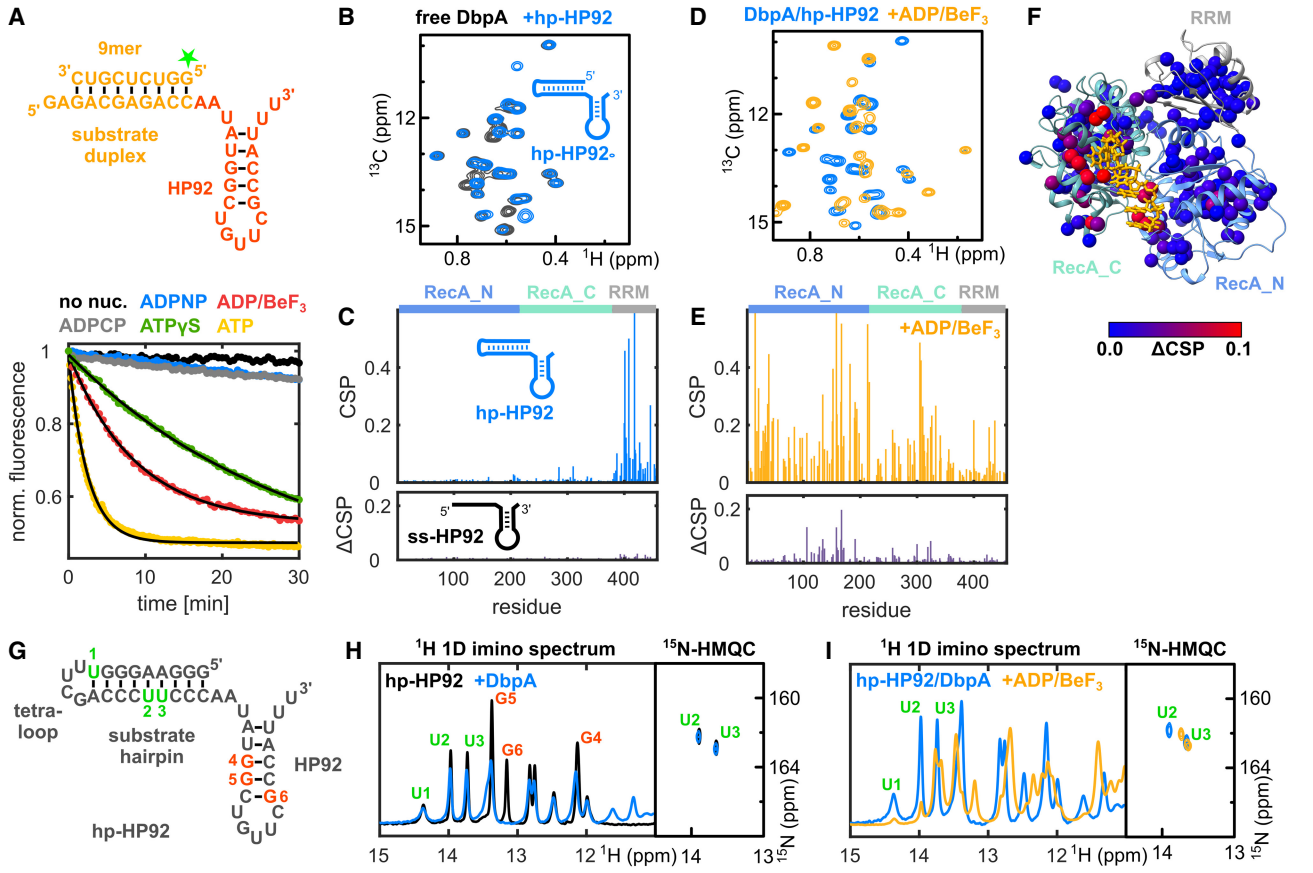

FIGURE 2. The DbpA/hp-HP92/ADPBeF$_3$ complex represents a trapped unwinding intermediate. (*A*) Fluorescence-based unwinding assays in the presence of different ATP analogs. A 5′ fluorescein (green star) labeled 9mer RNA is hybridized to an RNA containing HP92 (*top*). Unwinding can be followed by a decrease in fluorescence intensity (*bottom*). Mono-exponential fits to the fluorescence time traces are shown in black for ATP, ADP/BeF_3, and ATPγS. (*B*) Ile region of methyl TROSY spectra of ILMVA-labeled DbpA in the free state (black) and bound to hp-HP92 RNA (blue). (*C*) Sequence plots of chemical shift perturbations (CSPs) induced by binding of the hp-HP92 RNA (*top*) and differences between CSPs (ΔCSPs) induced by binding of the ss-HP92 RNA and the hp-HP92 (*bottom*). DbpA domains are indicated at the *top*. (*D*) Methyl TROSY spectra of DbpA/hp-HP92 complex prior to (blue) and after addition of ADP/BeF_3 (orange). (*E*) Sequence plots of CSPs induced by binding of ADP/BeF_3 to the DbpA/hp-HP92 RNA complex (*top*) and ΔCSPs between binding of ADP/BeF_3 to the ss-HP92/DbpA and to the hp-HP92/DbpA complexes (*bottom*). (*F*) ΔCSPs from (*E*) plotted onto a model of the closed state of DbpA bound to ssRNA (Wurm et al. 2021) (red, large ΔCSPs, blue, small ΔCSPs). The ssRNA is shown in orange. (*G*) Sequence of hp-HP92 RNA. Nucleotides with assigned imino proton signals are numbered and shown in red (HP92) or green (substrate hairpin). (*H*) ^{1}H-1D imino proton spectra (*left*) and ^{1}H^{15}N-HMQC spectra (*right*) of uridine ^{15}N-labeled hp-HP92 RNA prior to (black) and after addition of DbpA (blue). (*I*) Same spectra as in (*H*), but for the hp-HP92/DbpA complex prior to (blue) and after addition of ADP/BeF_3 (orange).

with a stable UUCG tetraloop was used as substrate (Fig. 2B). This substrate hairpin prevents the dissociation of the destabilized duplex. To probe the formation of the closed state, NMR titrations were performed using deuterated DbpA that is $^{1}H,^{13}C$-labeled at the methyl groups of Ile, Leu, Met, Val, Ala (ILMVA), and that yields high-quality methyl group spectra (Supplemental Fig. S3; Wurm et al. 2021). Binding of the hp-HP92 RNA substrate to DbpA can be monitored based on changes (chemical shift perturbations, CSPs) of the position of the methyl group signals (Fig. 2B; Supplemental Fig. S3). In the absence of ATP analogs, RNA binding induces large CSPs for residues that belong to the RRM, though only minimally affecting signals from the RecA core domains (Fig. 2C, upper graph). This demonstrates that only the RRM of DbpA interacts with HP92 of the hp-HP92 RNA, and that no specific contacts between the substrate duplex and the core domains are formed in the absence of ATP analog. In line with this, essentially identical CSPs are elicited by an RNA construct (termed ss-HP92) that contains a single-stranded region instead of the substrate duplex (Fig. 2C, bottom graph, note that differences in CSPs [ΔCSPs] are shown; Supplemental Fig. S4).

During the next step, the ATP analog ADP/BeF_3 was added to the DbpA/hp-HP92 complex. This leads to large CSPs within the helicase core domains (Fig. 2D,E, top graph; Supplemental Fig. S5). As we have shown previously (Wurm et al. 2021), these CSPs mark the formation of the DbpA closed state. Similarly, the closed state is also formed upon addition of ADP/BeF_3 to the DbpA/ss-HP92 complex (Supplemental Fig. S6). Interestingly, the DbpA spectra for the closed state reveal several distinct differences between ss-HP92 and hp-HP92 RNA complexes (Fig. 2E, bottom graph; Supplemental Fig. S6) and these differences cluster in the vicinity of the helicase core active site (Fig. 2F). I reasoned that these differences arise from the interaction with the intact substrate duplex in the hp-HP92 complex rather than the single-stranded region in the ss-HP92 RNA suggesting that the substrate duplex is not completely unwound in the hp-HP92/DbpA complex and that base-pairing persists within the RNA substrate despite the closed state of the enzyme.

To verify the base-pairing of the substrate duplex in the closed state, 1D ^{1}H imino proton spectra of the hp-HP92 RNA in isolation and in complex with DbpA were recorded (Fig. 2G–I). Only imino protons of nucleotides that are involved in stable base pairs give rise to observable signals in such spectra. To confirm the presence of the substrate hairpin, the signals of the three uridines within this hairpin (labeled U1–U3 in Fig. 2G,H) were used. Binding of DbpA in the absence ADP/BeF_3 only leads to a slight reduction in their signal intensity due to the increased molecular weight of the complex. This shows that there is no (or only a highly transient) interaction between DbpA and the substrate hairpin of the hp-HP92 RNA. In contrast, the guanosine residues of the HP92 stem (labeled G4–G6 in Fig. 2G, H) show clear CSPs due to direct interaction with the RRM of DbpA (Hardin et al. 2010; Wurm et al. 2021). The addition of ADP/BeF_3 to the DbpA/RNA complex leads to the formation of the closed state of DbpA and induces large shifts for essentially all imino proton signals (Fig. 2I). This provides clear evidence for a direct interaction between DbpA and the substrate hairpin within the closed state. At least seven to eight of the nine imino proton signals are still visible indicating that the substrate hairpin is still largely intact when bound to the active site of DbpA. This is supported by $^{1}H^{15}N$-HMQC spectra of uridine ^{15}N-labeled hp-HP92 RNA (Fig. 2I). In these spectra, only imino signals of base-paired uridines are detectable. The spectra show two uridine imino signals in the closed state, which must originate from the substrate duplex, as we have shown previously that the uridine imino signals of HP92 are not detectable under these measurement conditions (Wurm et al. 2021). These signals are thus tentatively assigned to the central uridines of the substrate hairpin (U2/U3).

In summary, these results demonstrate that the DbpA/hp-HP92/ADP/BeF_3 complex represents a trapped unwinding intermediate where the mostly intact duplex of the substrate hairpin interacts with the active site of the helicase core.

Structure of the hairpin RNA bound to the active site of DbpA

To understand how duplex destabilization by DbpA is achieved on a structural level, the crystal structure of the DbpA/hp-HP92/ADP/BeF_3 complex was solved to a resolution of 3.2 Å (Fig. 3A; Supplemental Table S1). Surprisingly, a domain swapped 2:2 DbpA:RNA complex is formed in the crystal. Each DbpA molecule interacts with the HP92 of one RNA molecule (via the RRM) and with the substrate hairpin (via the core domains' active site) of the other RNA. The two hairpins of each RNA molecule stack coaxially and HP92 is elongated by 2 bp, which are formed between the 3′ overhang of HP92 and the linker between HP92 and the substrate hairpin (nt 23–25; see Supplemental Fig. S7 for details and for a comparison between the HP92 RNA construct used for crystallization and the native RNA sequence of the 23S rRNA). Since the good quality of the NMR spectra (Fig. 2D) strongly argued against a 2:2 complex with a molecular weight >120 kDa, the oligomeric state of the DbpA/hp-HP92/ADP/BeF_3 complex in solution was investigated using size exclusion chromatography (SEC) experiments (Fig. 3C). The experiments show that addition of ADP/BeF_3 to the DbpA/hp-HP92 complex leads to the formation of two species: a minor population of a larger species, which is compatible with the 2:2 complex and a major population of a more compact species, which corresponds to the 1:1 complex. These results indicate that a 1:1 and a higher order complex (most likely the 2:2 complex observed in the

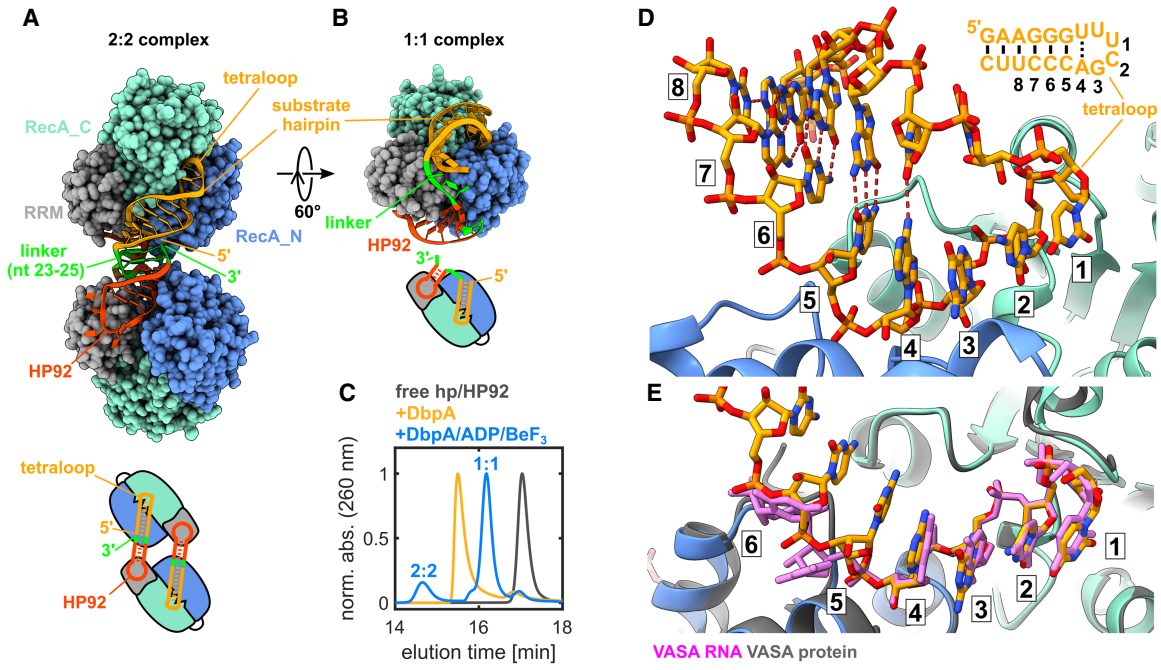

FIGURE 3. Crystal structure of the hp-HP92/DbpA complex in the closed state. (*A*) Overall structure (*top*) and schematic diagram (*bottom*) of the complex between two DbpA molecules (chains A/B) and two hp-HP92 RNAs (chains F/G), as observed in the crystal. HP92 (red), the substrate hairpin (orange), and the 3 nt linker that base pairs with the 3′ overhang of HP92 (green) are shown in ribbon representation. The RecA_N (blue), RecA_C (cyan), and RRM (gray) domains of DbpA are shown in sphere representation. (*B*) Model of the 1:1 complex obtained by connecting HP92 and the substrate hairpin bound to one DbpA molecule by a flexible 3 nt linker (green). (*C*) SEC chromatograms of free hp-HP92 (black), the hp-HP92/DbpA complex (orange), and the hp-HP92/DbpA/ADP/BeF_3 (blue) complex. (*D*) Close-up of the interaction between substrate hairpin (chain F, orange) and the active site of the helicase core (chain B, RecA_N blue, RecA_C cyan). The nucleotides that interact with the active site are numbered 1–6. The substrate hairpin is shown in the *upper-right*, with identical numbering. The distorted base pair between the adenosine in position 4 and the opposite uridine is indicated by a dashed line. (*E*) Comparison between the substrate hairpin bound to DbpA (only nt 1–7 are shown for clarity) and the complex between a 6 nt ssRNA (pink) and the DEAD-box helicase VASA (gray; PDB ID 2db3).

crystal structure) coexist in solution. The NMR experiments thus predominantly report on the major population of the 1:1 complex, whereas the minor population of the 2:2 complex was crystallized. Notably, the SEC and NMR experiments were conducted at similar concentrations, with higher concentrations used for crystallization trials, which is expected to increase the population of the 2:2 complex. Importantly, molecular modeling establishes that a 1:1 complex with identical DbpA/RNA interactions as observed for the 2:2 complex can be formed (Fig. 3B). I am thus confident that the observed interactions in the crystal structure between DbpA and the RNA hairpins are relevant in solution.

The interactions between HP92 and the RRM of DbpA are basically identical to the interactions observed for a homologous RRM/HP92 complex that was previously published (Supplemental Fig. S8; Hardin et al. 2010), and I hereby focus on the interaction between the substrate hairpin and the active site of the helicase core (Fig. 3D; Supplemental Fig. S9). The split active site interacts with 6 nt (numbered 1–6 in Fig. 3D) of the hairpin. The first 3 nt belong to the loop of the substrate hairpin, whereas nt 4–6 are part of the stem. Due to interaction with the active site, the first base pair of the stem (formed between the adenosine at position 4 and the opposing uridine) is distorted in comparison to a regular AU base pair, and consequently only forms one hydrogen bond. Conversely, the cytosines in positions 5 and 6 form regular GC base pairs with the opposing strand. All six bases in the binding site show continuous base stacking interactions.

Next, I compared the RNA conformation within the hp-HP92/DbpA complex with the canonical ssRNA product-bound state of other DEAD-box helicases (exemplified by the VASA helicase) (Fig. 3E; Sengoku et al. 2006). The conformation of nt 1–4 in both structures is basically identical. The main differences reside in the conformation of nt 5 and 6. In the VASA structure the bases of nt 5 and 6 are rotated by 90° relative to the DbpA structure and consequently their conformation is not compatible with duplex formation. In contrast to the known, product-bound states, this structure thus demonstrates that DbpA is able to bind a ss/dsRNA junction that contains a 5′ ssRNA overhang of 3 nt, whereby the 3 nt overhang and the first 3 nt of the duplex interact with positions 1–3 and 4–6 of the active site. I propose that the crystallized conformation represents a trapped unwinding intermediate that captures the

interaction between a ds/ssRNA junction and DbpA during unwinding.

Structure of a ss/dsRNA junction bound to the active site of DbpA

To exclude the possibility that the observed RNA conformation is influenced by the short loop of the substrate hairpin DbpA was crystallized in complex with a permuted RNA construct (termed ds-HP92) that contains a ss/dsRNA junction with a 3 nt 5′ overhang instead of the hairpin. To this end, the two coaxially stacking helices of the hp-HP92 RNA were fused, which places the 5′ and 3′ ends at the position of the loop of the substrate hairpin (Fig. 4A; Supplemental Fig. S7D). The complex crystallized as a 2:2 complex similar to the hp-HP92 RNA (Fig. 4A; Supplemental Fig. S7E), and the structure was determined to a resolution of 3.0 Å (Supplemental Table S1). Since fusion of the helices prevents the substrate duplex from folding back onto the active site of the same DbpA molecule, the 2:2 complex is also the major species in solution (Fig. 4B). In the structure, the 3 nt 5′ overhang and the first 3 nt of the substrate duplex are bound to the active site in positions 1–3 and 4–6, respectively (Fig. 4C; Supplemental Fig. S9B). The DbpA/RNA interactions are virtually identical to the ones observed in the hairpin structure, with the exception that the first base pair of the duplex (formed between the adenosine at position 4 and the opposing uridine) is not distorted. The distortion in the first base pair of the hp-HP92 RNA thus most likely originates from the strain in the short loop of the substrate hairpin.

To evaluate whether an extended duplex with base-paired nucleotides in positions 2 and 3 could interact with DbpA in a similar manner, two additional nucleotides at the 3′ end of the RNA were modeled in an A-form helix conformation (Fig. 4D, green residues). The model reveals that both nucleotides of the extended helix would severely clash with α-helix α7 of the RecA_N domain. This indicates that: (i) a 5′ single-stranded region of 3 nt is necessary for the interaction of duplex RNA with DbpA and (ii) only nucleotides in positions 4–6 can be part of a duplex, whereas positions 1–3 are not compatible with dsRNA. In summary, these results enforce the notion that DbpA interacts with a ds/ssRNA junction during the unwinding process, where nucleotides in positions 1–3 are single-stranded and nucleotides 4–6 can be part of a duplex.

Structure of the ssRNA product bound to the active site of DbpA

To complete the picture of the unwinding cycle of DbpA, I aimed to also gain insights into the ssRNA product-bound

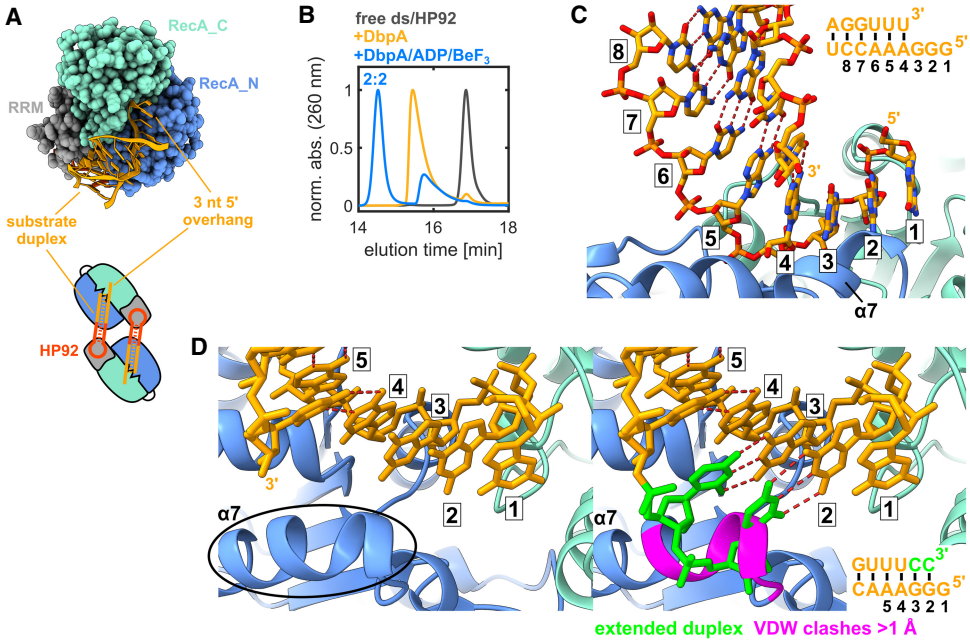

FIGURE 4. Crystal structure of the ds-HP92/DbpA complex in the closed state. (*A*) Interaction of the substrate duplex including a 3 nt 5′ overhang with the active site of the helicase core. For clarity, only the substrate duplex (chain D) and one DbpA molecule (chain B) are shown (*top*). Schematic diagram of the 2:2 complex observed in the crystal (*bottom*). (*B*) SEC chromatograms of free ds-HP92 (black), the ds-HP92/DbpA complex (orange), and the ds-HP92/DbpA/ADP/BeF_3 (blue) complex. (*C*) Close-up of the interaction between the substrate duplex (chain D, orange) and the active site of the helicase core (chain B, RecA_N blue, RecA_C cyan). The nucleotides that interact with the active site are numbered 1–6. The substrate duplex is shown in the *upper-right*, with identical numbering. (*D*) Close-up of the active site in the vicinity of α-helix α7 (*left*). Extension of the duplex by the addition of 2 nt at the 3′ end (green) leads to severe clashes with α-helix α7 of the RecA_N domain (*right*). Residues that show van der Waals clashes >1 Å with the RNA are shown in pink.

state after duplex unwinding. To this end, the structure of DbpA in complex with ADP/BeF_3 and an RNA construct termed ss-HP92 (Supplemental Fig. S7F) was solved. This RNA contains a single-stranded region 5′ to HP92 that interacts with the active site of the helicase core (Fig. 5A). Again crystallization resulted in a 2:2 RNA: DbpA complex (Supplemental Fig. S7G) and SEC experiments show that the 2:2 complex is predominant in solution (Fig. 5B). Similar to the ds-HP92 and hp-HP92 complexes, each DbpA molecule interacts with HP92 of one RNA via the RRM and with the single-stranded region of the other RNA via the core domains. Three 2:2 complexes are present in the asymmetric unit. All of them display highly similar structures. The main differences reside in the conformation of the single-stranded region of the RNA. Three RNAs (chains G, H, and L) adopt the same canonical ssRNA binding mode as observed in other DEAD-box helicases (conformation 1; Fig. 5C; Supplemental Fig. S9C). The bases of nt 1–4 show a continuous stacking interaction, whereas the bases of nt 5 and 6 are rotated by 90° relative to nt 1–4. In the other three RNAs (chains C, D, and K) all six bases show a continuous stacking interaction (conformation 2; Fig. 5D; Supplemental Fig. S9D). This continuous base stacking and the overall RNA conformation resembles the ds-HP92/DbpA complex structure (Supplemental Fig. S10). Conformation 2 could therefore represent a snapshot of the RNA conformation immediately following duplex dissociation, before the RNA transitions into conformation 1.

These results demonstrate that DbpA conforms to the canonical ssRNA product binding mode observed for other DEAD-box helicases, but also suggest a notable plasticity in its ssRNA interaction mode. A comparison between the ds-HP92 and ss-HP92 RNA-bound structures and the VASA/RNA complex shows that the interaction with nt 1–4 is essentially identical in all structures (Supplemental Fig. S11) and that the differences reside mainly in the interaction of nt 5 and 6 with the helicase core (Fig. 5E). In the canonical binding mode, the conserved R378 of VASA forms hydrogen bonds with the ribose of nt 5 and the phosphate group of nt 6. In the DbpA structures, the corresponding R132 is slightly repositioned, but forms similar interactions with nt 5 and 6. These results indicate that subtle structural differences in the conformation of R132 allow DbpA to favorably interact with the duplex as well as with ssRNA at positions 4–6.

Activity assays support an initial interaction with a ss/dsRNA junction during unwinding

In summary, the structures of the ds-HP92 and ss-HP92 complexes suggest the following model of duplex unwinding from a 5′ overhang. DbpA initially binds to the ss/

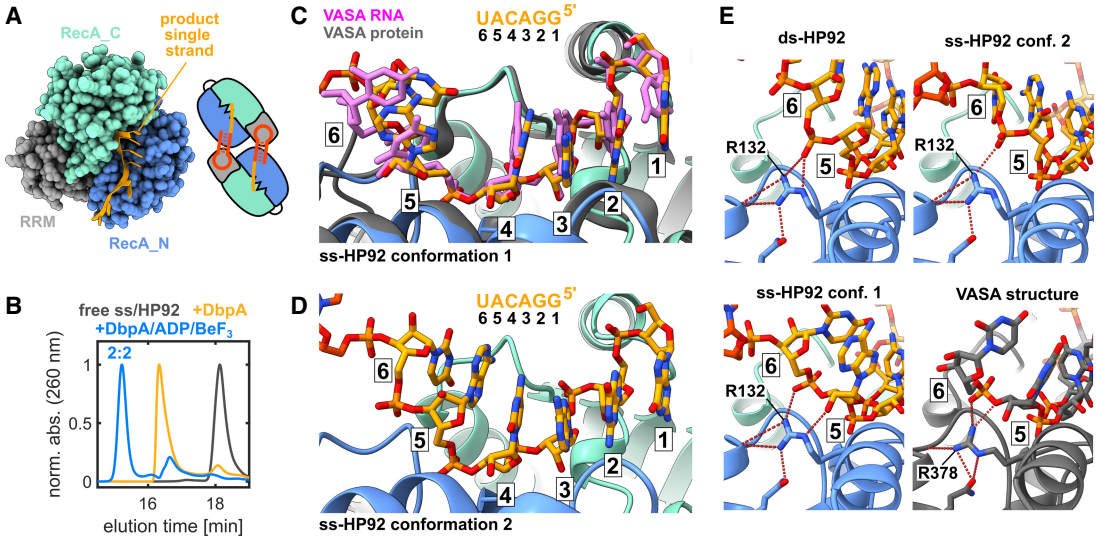

FIGURE 5. Crystal structure of the ss-HP92/DbpA complex in the closed state. (*A*) Interaction of the ssRNA with the active site of the helicase core. For clarity, only the ssRNA (chain L) and one DbpA molecule (chain I) are shown (*left*). Schematic diagram of the 2:2 complex observed in the crystal (*right*). (*B*) SEC chromatograms of free ss-HP92 (black), the ss-HP92/DbpA complex (orange), and the ss-HP92/DbpA/ADP/BeF_3 complex (blue). (*C*) Close-up of the interaction between the ssRNA region (chain L, orange) in conformation 1 and the active site of the helicase core (chain I, RecA_N blue, RecA_C cyan). For comparison, the complex between a 6 nt RNA (pink) and the DEAD-box helicase VASA (gray; PDB ID 2db3) is shown. The nucleotides that interact with the active site are numbered 1–6. The ssRNA sequence is shown on *top* with identical numbering. (*D*) Close-up of the interaction between the ssRNA region (chain C, orange) in conformation 2 and the active site of the helicase core (chain A, RecA_N blue, RecA_C cyan). (*E*) Comparison of the interactions between nucleotides in positions 5 and 6 for DbpA and VASA. The *top* row and the *bottom-left* panel show complexes between DbpA and ds-HP92 and ss-HP92 in conformation 1 and 2. The *lower-right* panel shows the VASA/ssRNA complex (PDB ID 2db3). Hydrogen bonds formed by R132 (DbpA) or the corresponding R378 (VASA) are indicated by dashed-red lines.

dsRNA junction of the duplex, where 3 nt of the 5′ overhang interact with positions 1–3 and the first 3 nt of the duplex with positions 4–6. Breathing of the duplex ends, which takes place on the ms timescale (Snoussi and Leroy 2001), thus leads to ss-HP92 conformation 2, and subsequently to ss-HP92 conformation 1. The ss-HP92 conformation 1 prevents duplex reformation, thereby destabilizing the remaining duplex and accelerating its spontaneous dissociation.

To validate this model, single-turnover unwinding assays with RNA constructs that contain a 9-bp duplex and a 5′ ssRNA overhang of 0, 2, 5, or 8 nt (Fig. 6A) were performed. The observed duplex unwinding rates (Fig. 6B) increase for overhangs of 0 and 2 nt from 0.20 min^{-1} to 0.42 min^{-1} and then decline for longer 5′ overhangs of 5 nt (0.32 min^{-1}) and 8 nt (0.21 min^{-1}). These results can be rationalized based on the model: The 5′ overhang of 0 nt shows the lowest unwinding rate, as the formation of the closed state depends on the presence of a 5′ single-stranded region. In the absence of a 5′ ssRNA overhang, this single-stranded region is only transiently formed by fraying of the terminal base pairs. Elongation of the overhang to 2 nt increases unwinding, as the overhang facilitates the formation of the closed state and only fraying of the terminal base pair is necessary. Longer overhangs are expected to facilitate the formation of the closed state even further, but also increase the risk of unproductive interactions, where DbpA would only bind to the ssRNA overhang, which would not destabilize the duplex region.

This finding is corroborated by ATPase assays with identical RNA constructs including the 9-bp duplex (Fig. 6C, red symbols). ATP hydrolysis requires formation of the closed state, and ATPase rates therefore report on the efficiency of closed state formation. The observed ATPase rates increase proportionally with 5′ overhang length from 2.3 min^{-1} for the 0 nt overhang to 52 min^{-1} for the 8 nt overhang, confirming that longer overhangs facilitate the formation of the closed state. Consequently, constructs with longer 5′ overhangs require additional ATP hydrolysis events for unwinding (Fig. 6D) as DbpA mainly forms unproductive closed states, where it binds to the 5′ ssRNA overhang remote from the RNA duplex. Based on this reasoning, ADP/BeF_3 should not support unwinding of duplexes with long 5′ overhangs, since DbpA should be trapped predominantly within unproductive closed states (note that a 5′ overhang of 2 nt was used in the helicase assays in Fig. 2A). This is experimentally verified in unwinding assays for the 8 nt 5′ overhang, where unwinding is strongly reduced compared to the 2 nt overhang (Fig. 6E). These results and the increased ATPase rate for longer 5′ overhangs indicate that DbpA does not favor the interaction with the ss/dsRNA junction over the interaction with the ssRNA 5′ overhang. To test this, ATPase assays were performed in the absence of the 9mer RNA, for the RNA carrying the 2 nt 5′ overhang (Fig. 6C, gray symbols). This leads to a 10.4-fold increase in the ATPase rate and indicates that formation of the closed state is even more favorable for a ssRNA substrate, compared to a ss/dsRNA junction. In summary, the observed helicase and ATPase rates are in good agreement with a model whereby DbpA preferentially forms the closed state upon interaction with a 5′ ssRNA overhang or a ssRNA/duplex junction, as observed in structures of the ss-HP92 and ds-HP92 complexes.

Transient active site formation and substrate RNA binding in the absence of ATP

Finally, I sought to gain direct insights into the initiation of the unwinding process, namely, the formation of the

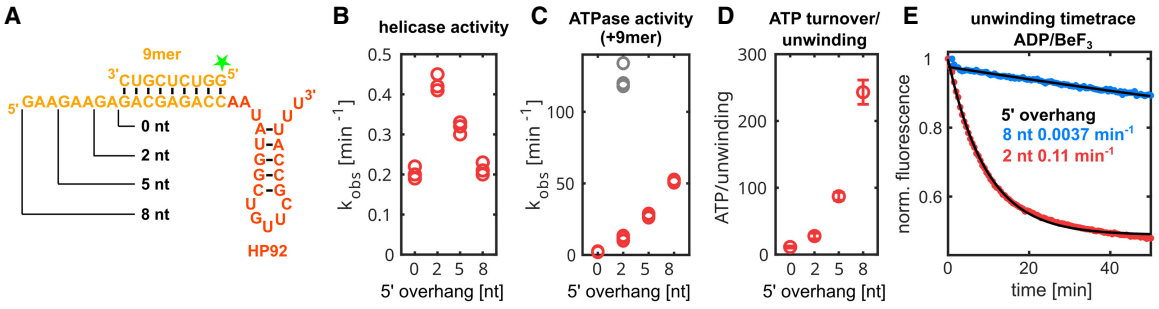

FIGURE 6. The length of the ssRNA 5′ overhang influences helicase and ATPase activity of DbpA. (*A*) RNA constructs used for activity assays. The substrate duplex (orange) is located 5′ to HP92 (red). The varying length of the 5′ overhangs is indicated. For helicase assays, the 9mer RNA contained a fluorescein label at the 5′ end (indicated by a green star). (*B*) Unwinding rates observed in single-turnover experiments are plotted versus the 5′ overhang length. Results from three measurements are shown. (*C*) ATPase turnover rates are plotted versus the 5′ overhang length. Rates were determined in the absence (gray) and presence of the 9mer RNA (red). Results from three measurements are shown. (*D*) The number of hydrolyzed ATP molecules for each unwinding event are plotted versus the 5′ overhang length. The values represent mean and standard deviation calculated from the experiments shown in panels *B* and *C*. (*E*) Single-turnover unwinding of RNA constructs with a 5′ overhang of 2 nt (red) or 8 nt (blue) in the presence of ADP/BeF_3 is followed by fluorescence intensity measurements. Exponential fits to fluorescence time traces are shown in black and the unwinding rates obtained from the fits are given.

closed state. Closing of the DbpA/RNA complex is inherently inefficient as three bodies (the two RecA domains and substrate RNA) require assembly in the correct orientation. This raises the question whether the substrate RNA binds to a preformed active site (where the two RecA domains assemble initially) or whether the substrate RNA initially interacts with one of the RecA domains prior to the active site assembly. To test for active site preformation, paramagnetic relaxation enhancement (PRE) experiments were performed using an RNA construct that corresponds to isolated HP92 (Fig. 7A; Supplemental Fig. S12A) and that carries a nitroxide spin label at the 3′ end. The spin label induces a PRE that leads to a strong decrease of the methyl group NMR signals in its vicinity, which can be readily quantified and allow for the detection of sparsely populated states (Clore et al. 2007). Upon binding of the spin labeled HP92, the expected PREs close to the HP92 binding site on the RRM are observed. Additional PREs are observed on top of the RecA_N domain (Fig. 7A; Supplemental Fig. S12A) indicating that this region of the RecA_N domain also approaches the spin label. Since close contacts between the RecA_N domain and HP92 are only found in the closed state of the enzyme (Fig. 7A), these results clearly indicate that DbpA transiently adopts the closed state in the presence of HP92. It would be interesting to explore whether the closed state is also formed in the absence of HP92. However, due to the nine native cysteine residues in DbpA site selective spin labeling of DbpA was not possible.

To test for interactions between the substrate duplex and the RecA domains, the PRE experiments were repeated with a hp-HP92 RNA construct that carries a spin label in the loop of the substrate hairpin (Fig. 7B; Supplemental Fig. S12B). In the absence of ATP analog, the PREs for this RNA construct are distributed over a large surface on the RRM and RecA_C domains, indicating that the substrate hairpin only transiently interacts with these domains, and samples a large set of different conformations. The largest PREs are observed for a positively charged region

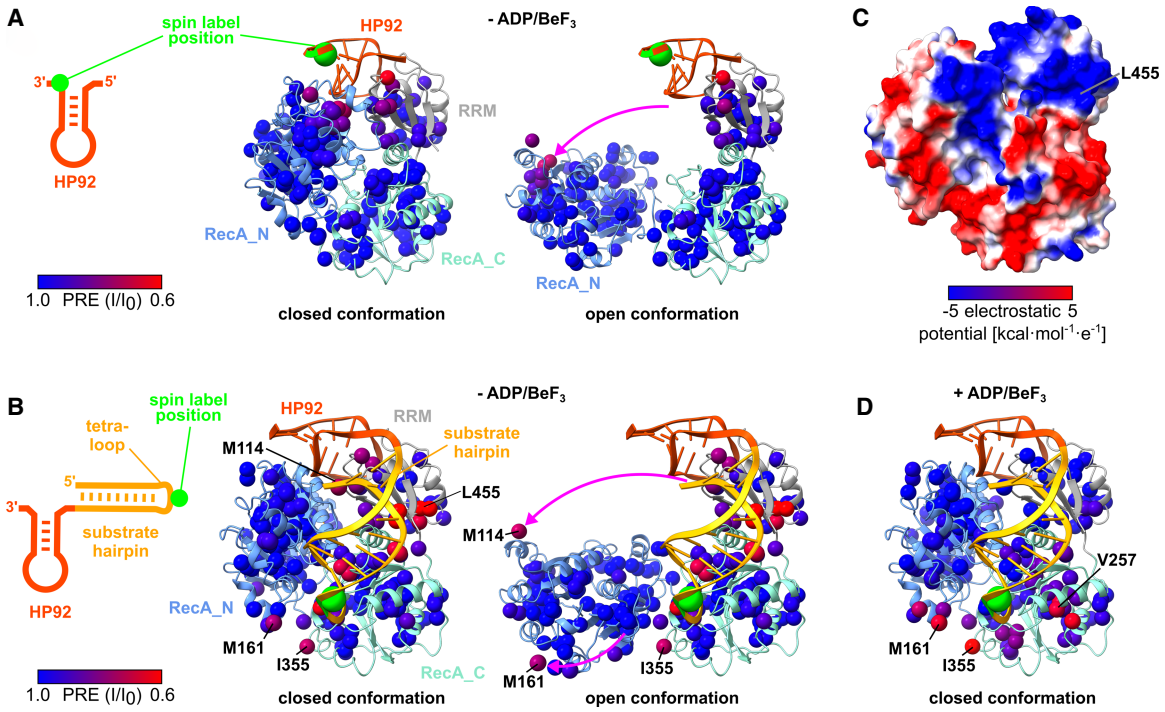

FIGURE 7. DbpA transiently samples the closed state in the absence of ATP. (*A*) PRE experiments were performed with spin labeled HP92 RNA and ILMVA-labeled DbpA in the absence of ADP/BeF_3. The RNA construct is shown on the *left*. The position of the 4-thiouridine residue that carries the nitroxide spin label is indicated by a green circle. The methyl groups of DbpA are colored according to the decrease in signal intensity, due to the spatial proximity of the spin label from blue (no effect) to red (strong reduction). The closed conformation (*left* structure) and an arbitrary open conformation (*right* structure) are depicted. The pink arrow indicates the reorientation of the RecA_N domain between the two structures. The C1′ atom of the spin labeled 4-thiouridine is shown as a green sphere. (*B*) PRE experiments with an hp-HP92 RNA containing a spin label in the loop of the substrate hairpin (green circle; *left*). Methyl groups are colored as in (*A*) for the closed conformation (*left* structure) and for an arbitrary open conformation (*right* structure). The pink arrows indicate the reorientation of the RecA_N domain. The methyl groups of M114 and M161 that exhibit the largest PREs in the RecA_N domain are labeled. The RNA is shown in the conformation observed in the DbpA/hp-HP92 complex, where the substrate interacts with the active site of the helicase core. (*C*) DbpA in the closed conformation colored according to its electrostatic surface potential (blue = positive, red = negative). (*D*) PRE experiments with identical RNA as in (*B*), but in the presence of ADP/BeF_3. Methyl groups are colored as in (*A*) and DbpA is shown in the closed conformation.

on the RRM surrounding L455 (Fig. 7C). This positively charged patch is located remotely from the active site, and its function is currently unknown. It was speculated to be important for RNA interactions in the context of the preribosome (Hardin et al. 2010) and most likely attracts the substrate hairpin in the PRE experiments due to its positive charge. More importantly, the residues from the RecA_N domain with the largest PREs (M114 and M161) and the residues with large PREs on the RecA_C domain are in closer contact in the closed conformation (Fig. 7B): e.g., for M114/M161 the distance to the spin label decreases from 54/42 Å (open state) to 27/18 Å (closed state). This indicates that DbpA also transiently adopts the closed conformation in the presence of hp-HP92 and thereby corroborates the results for the isolated HP92 (Fig. 7A). In addition to M161 from the RecA_N domain, large PREs are also found for I355 from the RecA_C domain. Both residues are located in the proximity of the spin label when the substrate hairpin is bound to the active site in the closed state (Fig. 7B). These PREs therefore suggest that the transiently formed, closed state interacts with the substrate hairpin in a similar manner as observed in the structure of the stably closed hp-HP92/DbpA complex. In line with this finding, large PREs are observed for M161 and I355 upon stable formation of the closed state by addition of ADP/BeF_3 (Fig. 7D; Supplemental Fig. S12C). These PREs are also in good agreement with the structure of the hp-HP92/DbpA complex and thereby provide an independent validation of this structure.

Overall, the PRE experiments demonstrate the transient formation of the closed state in the presence of HP92 and hp-HP92 RNAs, and also suggest that the substrate hairpin interacts with the transiently formed active site in a similar manner as observed in the hp-HP92/DbpA structure. This hints at a pathway for the formation of the active state, where the closed state is transiently formed and, consequently, the substrate duplex is recruited to the preformed active site in a second step.

DISCUSSION

The crystallographic snapshots of the unwinding intermediates that I determined in this study fill a major gap in our understanding of the unwinding process of DEAD-box helicases and rationalize how the destabilization of the RNA duplex in the closed state is achieved. Note that HP92 is not included in the following model as HP92 is not directly involved in the unwinding mechanism discussed here. Instead, HP92 is necessary for the stabilization of the closed state, which also rationalizes its in-trans activation of the unwinding process (Wurm et al. 2021). The structures obtained in this study can be readily integrated into a model of the unwinding process (Fig. 8): Prior to binding of the substrate duplex, DbpA mainly populates an open state, whereby the RecA_N domain tumbles independently from the other two domains. This open state, however, transiently adopts the closed conformation. In the first step (1), the RNA duplex is recruited to this transiently formed, closed conformation. DbpA initially binds to 3 nt of the 5′ overhang and the first 3 nt of the substrate duplex, as depicted in the ds-HP92 complex structure (Fig. 4). Breathing of the duplex ends in the active site (step 2), which takes place on the μsec–msec timescale (Snoussi and Leroy 2001), leads to conformation 2 of the ss-HP92 complex (Fig. 5D). In this conformation, all residues still exhibit a continuous base stacking. Subsequently, in step (3), a transition to the canonical ssRNA product conformation (as observed in conformation 1 of the ss-HP92 complex) (Fig. 5C) prevents reformation of the 3 bp. This strongly destabilizes the remaining duplex and increases the dissociation rate for the unbound RNA strand (step 4). The number of destabilized base pairs predicted based on these considerations is also in fair agreement with the number obtained from functional assays for the DEAD-box helicases eIF4A and Ded1 (2–3 and 4–5 bp, respectively; Rogers et al. 1999; Raj et al. 2019).

Importantly, this model depicts only one of several different unwinding pathways that are compatible with the results of this study. DbpA forms the closed state even more efficiently in the presence of ssRNA compared to the ss/dsRNA junction (Fig. 6C). It is therefore very likely that it can also bind more distal to the duplex such that only 1 or 2 nt of the duplex interact with the active site of the helicase core. Regarding blunt-end duplexes, fraying of the duplex ends will expose the 5′ ssRNA overhang that is necessary for binding. As HP92 does not need to be attached to the substrate duplex to support unwinding, a precise positioning of the duplex by HP92 is not essential for the unwinding process. It is also important to note that in my experiments the attachment of the substrate duplex to HP92 enforces the interaction with the duplex end that is distant from the HP92 attachment site and prevents interaction with the proximal duplex end that carries a 3′ overhang. This study therefore only provides insights into unwinding from the distant duplex end that carries the 5′ ssRNA overhang.

For most DEAD-box helicases, the unwinding activity strongly increases with 3′ and with 5′ ssRNA overhangs relative to blunt-end duplexes (Linder and Jankowsky 2011), indicating that DEAD-box helicases can also effectively initiate unwinding from 3′ ssRNA overhangs. This must proceed through a different mechanism, which might be analogous to the one described here and would involve binding to a ss/dsRNA junction with a 3′ ssRNA overhang. In this case, the duplex region would bind to positions 1–3, which are mainly formed by the RecA_C domain, and the 3′ ssRNA overhang would interact with positions 4–6. This notion is supported by the structure of the isolated RecA_C domain of the DEAD-box helicase

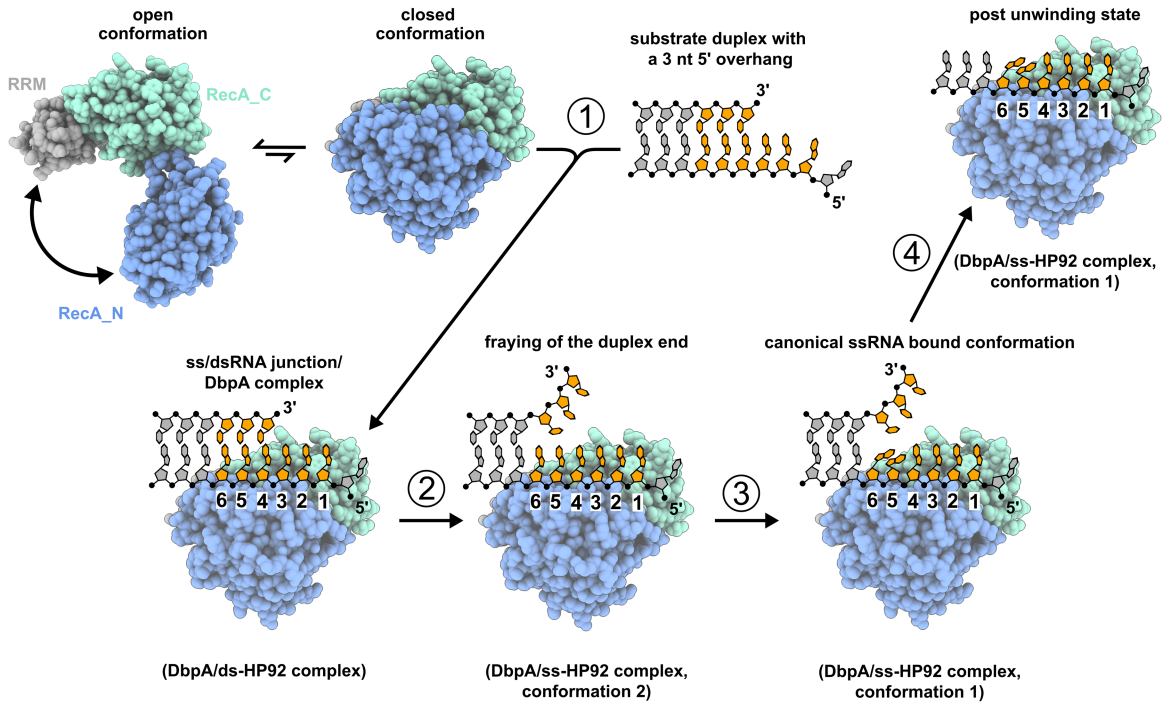

FIGURE 8. Model of the unwinding mechanism for duplexes with 5′ ssRNA overhangs. HP92 and ATP are omitted for clarity. The nucleotides that interact with the active site of DbpA are colored orange. DbpA transiently adopts the closed conformation in the absence of substrate RNA (*upper left*). (1) The closed conformation binds to the ss/dsRNA junction, whereby nt 1–3 are single-stranded and nt 4–6 are still part of the duplex (as depicted in the structure of the DbpA/ds-HP92 complex). (2) Duplex breathing leads to a ssRNA-bound state with continuous base stacking (DbpA/ss-HP92 complex in conformation 2). (3) The nucleotides in positions 5/6 rearrange to a conformation that is incompatible with duplex formation (DbpA/ss-HP92 complex in conformation 1). (4) The loss of these three base pairs leads to the dissociation of the upper RNA strand.

Mss116 in complex with an RNA duplex, which shows that duplex binding to positions 1–3 is also possible (Mallam et al. 2012).

Interestingly, the ATPase assays with increasing 5′ overhangs indicate no specificity of DbpA for the ss/dsRNA junction over ssRNA. 5′ ssRNA overhangs of increasing length are detrimental to the unwinding process. This is in agreement with previous reports on DbpA (Henn et al. 2010) and a similar observation has been made for the DEAD-box helicase eIF4A (Andreou et al. 2019). These findings support a model where DEAD-box helicases act as ATP-fueled ssRNA binding proteins, rather than dsRNA-specific helicases. In this scenario, unwinding would be the result of stochastic binding to ss/dsRNA junctions, rather than a process that is targeted toward RNA duplexes. In line with this proposed lack of duplex-specificity, most DEAD-box helicases show strongly increased ATPase activity in the presence of ssRNA (Putnam and Jankowsky 2013), indicating that interaction with a duplex is generally not necessary for the formation of the closed state. In addition, several DEAD-box helicases have been shown to act as ssRNA clamps (Ballut et al. 2005; Xiol et al. 2014) or in the remodeling of RNA/protein complexes (Bowers et al. 2006; Tran et al. 2007), and these two processes are unrelated to the interaction with dsRNA. In line with prior suggestions (Liu et al. 2008), I therefore favor a simple model, where the functions of DEAD-box helicases are explained by ATP-coupled, high-affinity ssRNA (or ss/dsRNA junction) binding.

In summary, these results indicate that for DbpA unwinding of duplexes with a 5′ ssRNA overhang proceeds through binding of the helicase core to the 5′ ss/dsRNA junction. The high conservation of the characteristic DEAD-box sequence motifs in DbpA (Supplemental Fig. S13; Putnam and Jankowsky 2013), together with the similarity of the ssRNA product-bound structure (ss-HP92 conformation 1) to the canonical product-bound state of DEAD-box helicases (Fig. 5C) suggests that the results can be generalized to other DEAD-box helicases. Nonetheless, in addition to the unwinding pathway via the 5′ ss/dsRNA junction described here, several other pathways are possible and remain to be described.

MATERIALS AND METHODS

Protein expression and purification

For DbpA expression the gene coding for full-length DbpA (UniProt accession code P21693) was PCR amplified from *E. coli* BL21 (DE3) genomic DNA and cloned into a pETM-11 plasmid that

codes for an N-terminal tobacco etch virus (TEV) protease cleavable hexahistidine tag. This plasmid was transformed into *E. coli* BL21(DE) codon plus cells. All growth media for protein expression were supplemented with 50 mg/L kanamycin and 34 mg/L chloramphenicol. Cells were grown in LB medium at 37°C until an OD_{600} of 0.6–0.8 was reached. For the production of unlabeled DbpA, protein expression was induced at this stage by the addition of 1 mM IPTG, the cells were shifted to 25°C and harvested after 16–20 h. For the production of the ILMVA methyl group labeled DbpA, 1 mL of the LB culture was used to inoculate 25 mL of H_2O-based M9 minimal medium and cells were grown to an OD_{600} of 0.6–0.8. Cells were harvested by centrifugation and used to inoculate 100 mL of D_2O-based M9 medium (containing 4 g/L deuterated glucose) at an OD_{600} of 0.15. Cells were grown overnight at 37°C and diluted 1/8 with fresh D_2O-based M9 medium (containing 2 g/L deuterated glucose) in the morning. Cells were grown at 37°C until an OD_{600} of 0.8 was reached. The culture was shifted to 25°C and 60 mg 2-ketobutyric acid-(4-^{13}C,3,3-d_2), 100 mg 2-keto-3-methyl-butyric acid-(dimethyl-$^{13}C_2$, 3-d), and 100 mg L-methionine-(methyl-^{13}C) dissolved in 200 mL of D_2O-based M9 medium were added. After 45 min, 100 mg L-alanine-(methyl-^{13}C, 2-d) was added and 15 min later protein expression was induced by addition of 1 mM IPTG. Cells were harvested after 16–20 h and stored at −20°C.

For purification, the cell pellets were resuspended in 20 mL of buffer A (400 mM NaCl, 50 mM sodium-phosphate, pH 7.4, 10 mM imidazole) supplemented with 0.1% (v/v) Triton-X-100, 1 mg/mL lysozyme, and 0.1 mg/mL DNase I. Cells were lysed by sonication and cell debris was removed by centrifugation (30 min, 18,000*g*, 4°C). The supernatant was applied to a gravity flow Ni-NTA column equilibrated in buffer A. The column was washed with 20 mL of buffer A, 10 mL of 1 M NaCl, 25 mM sodium-phosphate, pH 7.4, and 20 mL of buffer A + 10 mM imidazole. DbpA was eluted with buffer B (400 mM NaCl, 300 mM imidazole, 50 mM sodium-phosphate, pH 7.4). The N-terminal His-tag was removed by TEV protease digestion during dialysis against dialysis buffer (150 mM NaCl, 25 sodium-phosphate, pH 7.4, 1 mM DTT) overnight at 4°C. The TEV protease contained an N-terminal hexahistidine tag and was removed by a second Ni-NTA column equilibrated in dialysis buffer. The column was washed with dialysis buffer. Flow-through and wash fractions were combined and ½ volume of 60% (v/v) glycerol solution was added. DbpA was further purified using a 5 mL HiTrap HP Heparin column (GE Healthcare) equilibrated in 100 mM NaCl, 20 mM HEPES, pH 7.3, 20% (v/v) glycerol. DbpA was eluted using a linear NaCl gradient from 100 mM to 500 mM over 50 mL. DbpA-containing fractions were pooled, concentrated, and subjected to a size exclusion chromatography (SEC) step using a Superdex 75 16/600 column (GE Healthcare) equilibrated in SEC buffer (125 mM NaCl, 25 mM HEPES, pH 7.3, 1 mM DTT). DbpA concentrations were determined based on the OD_{280} using an extinction coefficient of 26,900 M^{-1} cm^{-1}.

RNA production

RNAs were produced by in vitro transcription (IVTC) using homemade T7 polymerase (P266L mutant) (Guillerez et al. 2005). Single-stranded DNA oligonucleotides, to which a DNA oligonucleotide corresponding to the T7 promotor sequence was hybridized, were used as templates. IVTCs were performed in 5–10 mL reactions containing 1 µM template DNA, 4 mM of each NTP, 15–50 mM $MgCl_2$ (optimized for each RNA construct), 50 mM Tris, pH 8.0, 1 mM spermidine, 5 mM DTT, 0.01% (v/v) Triton-X-100, 40 µg/ml T7 polymerase and were incubated at 37°C for 3 h. Subsequently, 50 mM EDTA, pH 8.0 was added, and the RNA was precipitated by addition of 0.7 volumes of isopropanol. RNAs were purified using a DNAPac 100 column (22 × 250 mm, Dionex) heated to 70°C. Buffers for purification contained 5 M urea, 20 mM Tris, pH 8.0 (pH adjusted at RT) and 0 (buffer A) or 2 M NaCl (buffer B). RNAs were eluted using linear gradients from 5%–15% B to 20%–40% B depending on the RNA construct at a flow rate of 10 mL/min. Fractions containing the desired RNA product were pooled and precipitated by addition of 1 volume of isopropanol and incubation at −20°C for at least 1 h. After centrifugation (8000*g*, 4°C, 45 min), the RNA pellet was washed with 75% (v/v) ethanol, dried and resuspended in H_2O. RNA concentrations were determined based on OD_{260}. Extinction coefficients were calculated using the OligoAnalyzer Tool (IDT). See Supplemental Table S2 for the sequences of the RNA constructs used in this study.

NMR experiments

All NMR experiments were conducted on Bruker 600 MHz and 800 MHz Avance Neo spectrometers equipped with nitrogen (600 MHz) or helium cooled (800 MHz) cryoprobes. Methyl TROSY spectra were recorded using the SOFAST-HMQC pulse sequence (Schanda et al. 2005). Measurements were performed at 25°C in SEC buffer supplemented with 5% (v/v) D_2O for the lock. DbpA concentrations in titration experiments with ILMVA-labeled DbpA were 40–70 µM, and RNAs were added in 1.3 times excess over DbpA. For experiments where RNAs where titrated with DbpA, RNA concentrations were 100 µM and unlabeled DbpA was added in 1.3 times excess over RNA. To form the ADP/BeF_3 bound state 2 mM $MgCl_2$, 2 mM BeF_2, 2 mM ADP, and 10 mM NaF were added. CSPs were calculated according to the following equation:

$$\mathrm{CSP} = \sqrt{(\Delta C/4)^2 + \Delta H^2}$$

(ΔC, ΔH, chemical shift differences in ppm in the ^{13}C and ^{1}H dimensions).

Methyl group assignments in the free and RNA-bound states of DbpA were published previously (Wurm 2020; Wurm et al. 2021). Assignments for the RNA-bound state could be partially transferred to the closed state (bound to ss-HP92 RNA and ADP/BeF_3) based on 3D-NOESY spectra in combination with the structure of the DbpA/ss-HP92/ADP/BeF_3 complex. The sample for the NOESY spectra contained the 250 µM ILMVA methyl group labeled DbpA, 350 µM ss/HP92 RNA, 110 mM NaCl, 25 mM Arg/Glu, 25 mM HEPES, pH 7.3, 1 mM DTT, 5 mM $MgCl_2$, 2 mM ADP, 4 mM BeF2, and 15 mM NaF. SOFAST-HMQC-based 3D-CCH- and 3D-HCH-NOESY spectra (Rossi et al. 2016) were recorded with a mixing time of 250 msec.

Imino proton signals of the substrate duplex of the hp-HP92 RNA in the free state were assigned using a 2D ^{1}H-^{1}H NOESY spectrum (mixing time 130 msec) recorded in SEC buffer at 10°C at an RNA concentration of 200 µM. The assignment of

the imino protons of HP92 was published previously (Wurm et al. 2021).

NMR spectra were processed with Topspin 4.0.2 or NMRPipe 9.6 (Delaglio et al. 1995) and analyzed using NMRPipe and CARA (Keller 2004).

PRE measurements

RNAs for site selective spin labeling contained a 4-thiouridine at the desired labeling position and were chemically synthesized by Dharmacon, see Supplemental Table S2 for RNA sequences. RNAs were deprotected according to the protocol provided by Dharmacon. For spin labeling, 100 µM of the respective RNA was incubated at room temperature in the dark for 24 h with a 100-fold excess of 4-(2-iodoacetamido)-TEMPO in a buffer containing 20% (v/v) DMSO and 100 mM HEPES, pH 8.0. Unreacted 4-(2-iodoacetamido)-TEMPO was removed by two sodium acetate/EtOH precipitation steps. PRE experiments were performed in NMR buffer lacking DTT using a 1.3 times excess of RNA over DbpA. DbpA concentrations ranged from 40 µM to 60 µM. SOFAST-HMQC spectra were recorded before and after reduction of the spin label by addition of 2 mM sodium ascorbate. Peak volumes in both spectra were integrated with NMRPipe and the PRE was calculated as the ratio of the peak volumes before reduction (I) divided by the peak volumes after reduction (I_0). PRE values for the geminal methyl groups of Leu and Val residues were averaged.

Helicase assays

Fluorescence-based single-turnover helicase assays were conducted at 25°C in 96-well plates using a TECAN spark plate reader. The assay takes advantage of the fluorescence quenching effect of the 5′ guanosine residues of the 9mer RNA on the 5′ fluorescein label. This effect is strongly reduced, when the labeled 9mer is hybridized to the HP92 containing RNA and leads to a reduction of the fluorescence intensity upon unwinding. Rebinding of the 9mer RNA to HP92 containing RNA is prevented by an excess of unlabeled 9mer RNA. See Supplemental Table S2 for RNA sequences. 5′ fluorescein labeled RNAs were obtained from IDT. Reaction mixtures (100 µL) contained 125 mM NaCl, 25 mM HEPES, pH 7.3, 2 µM DbpA, 5 mM $MgCl_2$, 25 nM 5′ fluorescein labeled 9mer RNA, 37.5 nM HP92 containing RNA, 2 µM unlabeled 9mer RNA, 3 mM of the respective nucleotide (ADP, ATP, ADPNP, ADPCP, or ATPγS). For the ADP/BeF_3 condition, 3 mM BeF_2 and 10 mM NaF were added in addition to ADP. Initially, 5′ fluorescein labeled 9mer RNA (at 1 µM) and HP92 containing RNA (at 1.5 µM) were hybridized in SEC buffer supplemented with 5 mM $MgCl_2$ by heating to 95°C and subsequent cooling to room temperature over ~1 min. Then all components except for the nucleotide were mixed and preincubated for 5 min in the plate reader. The unwinding reaction was started by the addition of nucleotide (+BeF_2 and NaF in the case of the ADP/BeF_3 condition) and the fluorescein fluorescence (excitation/emission filter wavelength 485 nm/535 nm) was recorded every 30 sec. Fluorescence time courses were fitted to the following equation:

$$F = F_0 + \Delta F \cdot e^{-kt}$$

(F, fluorescence intensity; F_0, basal fluorescence intensity; ΔF, fluorescence intensity difference due to unwinding; k, unwinding rate; t, time) using Matlab. All helicase assays were performed in triplicate using the same DbpA preparation, which was stored in small aliquots at −80°C until use. The reported values are the mean and standard deviation of the three measurements.

ATPase assays

The ATPase activity of DbpA in the presence of different RNA constructs was determined using a coupled pyruvate kinase/lactate dehydrogenase assay (Tsu and Uhlenbeck 1998; Kiianitsa et al. 2003). The production of ADP is coupled to NADH oxidation, which can be monitored based on NADH absorption at 340 nm. Reaction mixtures (150 µL) contained 0.2–1 µM DbpA, 3 mM ATP, 5 µM HP92 containing RNA, 0 or 6.5 µM 9mer RNA, 450 µM NADH, 1.5 mM pyruvate, 10 u/mL pyruvate kinase/lactate dehydrogenase (from rabbit muscle, Sigma-Aldrich, #P0294), and 5 mM $MgCl_2$ in SEC buffer. Absorption measurements at 340 nm were conducted in 96-well plates every 20 sec using a TECAN spark plate reader at 25°C. ATPase rates were determined based on the following equation after linear fitting of the linear region of the absorption time courses:

$$k_{obs} = -\frac{dA}{dt} \cdot \left(\frac{1}{K_{path} \cdot [DbpA]} \right)$$

(k_{obs}, ATPase activity; dA/dt, slope of the linear fit to the absorption time course; K_{path}, molar absorption coefficient of NADH at 340 nm for the path length in the 96-well plate [2.22 mM^{-1}]; [DbpA], DbpA concentration). All ATPase assays were performed in triplicate using the same DbpA preparation, which was stored in small aliquots at −80°C until use. The reported values are the mean and standard deviation of the three measurements.

Structure modeling

Structure modeling was performed in torsion angle space using CYANA 3.98 (Güntert et al. 1997). The 1:1 complex between hp-HP92 RNA and DbpA was modeled based on chain B (DbpA), nt 1–22 of chain F and nt 26–42 of chain G. The torsion angles in these residues were fixed (except for the ε backbone angle of nt 22 and the α, β, δ, and ζ backbone angles of nt 26) and nt 23–25 of the hp-HP92 were modeled to connect chains F and G using the regularize macro implemented in CYANA. Fifty structures were calculated and the structure with the lowest target function was chosen to represent the model.

To model the elongated duplex of the ds-HP92 RNA (Fig. 4), two cytosine residues (corresponding to nt 45 and 46) were added to the 5′ end of the ds-HP92 RNA. For these cytosines, A-form helix restraints (Richardson et al. 2008) and Watson–Crick hydrogen bond restraints to nt G2/G3 were introduced. All angles of the ds-HP92 RNA except for the δ and ε backbone angles of nt 44 were fixed. Fifty structures were calculated by simulated annealing and the structure with the lowest target function was chosen to represent the model.

Analytical size exclusion chromatography

Analytical SEC of RNA and RNA/DbpA complexes was performed at 25°C using an XBridge Protein BEH SEC 200 Å

Column (7.8 mm × 300 mm) and SEC buffer (flow rate 0.5 mL/min). RNAs were folded by heating the RNAs at a concentration of 80 µM in SEC buffer to 95°C for 1 min, followed by rapid cooling on ice. Five microliters of solution containing RNA at a concentration of 40 µM in SEC buffer were injected for each run. DbpA was added at a 1.3-fold excess and 2 mM ADP, 2 mM BeF_2, 2 mM $MgCl_2$, and 10 mM NaF were added to form the RNA/DbpA/ADP/BeF_3 complexes. The RNA/DbpA/ADP/BeF_3 complex was incubated at least 20 min at room temperature before analysis. RNA elution was monitored by recording the absorption at 260 nm.

Crystallization and structure determination

The DbpA/RNA/ADP/BeF3 complexes for crystallization were prepared in SEC buffer using DbpA and RNA concentrations of 200 µM and 260 µM, respectively. Before mixing with DbpA, RNAs were folded at a concentration of 700 µM in H_2O by heating to 95°C for 1 min followed by rapid cooling on ice and subsequent addition of NaCl to a final concentration of 125 mM. Then 3 mM ADP, 5 mM BeF_2, 5 mM $MgCl_2$, and 16 mM NaF were added and the complex was incubated at least 1 h at room temperature before crystallization. Crystals were grown using the hanging drop vapor diffusion method at 20°C after mixing 1 µL of the complex solution with 1 µL of the reservoir solution. Crystals appeared after 1–2 d. Crystals were cryoprotected using reservoir solution + 20% (v/v) PEG400 and subsequently flash frozen in liquid nitrogen. The following reservoir solutions were used:

hp-HP92RNA: 200 mM NH_4/tartrate, 100 mM Tris, pH 8.0, 20% (w/v) PEG3350

ds-H92 RNA: 0.2 M di-sodium tartrate, 20% (w/v) PEG 3350

ss-HP92 RNA: 400 mM KSCN, 100 mM Tris, pH 8.0, 20% (w/v) PEG 3350

Diffraction data were collected at −170°C and at a wavelength of 0.9766 Å at the EMBL/DESY beamline P13 (Cianci et al. 2017) (for the ss/HP92 RNA/DbpA complex) or at a wave length of 1.000 Å at the SLS beamline X06SA (Mueller et al. 2012) (for the hp/HP92 and ds/HP92 RNA/DbpA complexes). The collected data was integrated, merged, and scaled using XDS (Kabsch 2010). Phasing of the hp-HP92 RNA complex was performed by molecular replacement using PHASER (McCoy et al. 2007) and the structures of the DEAD-box helicase VASA (PDB 2DB3) (Sengoku et al. 2006) and of the RRM of the DbpA homolog YxiN (PDB 3MOJ) (Hardin et al. 2010) as search models. For the other two complexes, the DbpA structure of the hp-HP92 RNA complex was used as a molecular replacement search model. The structures were refined by iterative rounds of manual model building in COOT (Emsley and Cowtan 2004) and refinement using Phenix.refine (Afonine et al. 2012). Data collection and refinement statistics are summarized in Supplemental Table S1. Structure representations were generated with UCSF ChimeraX (Pettersen et al. 2021).

DATA DEPOSITION

Structure factors and atomic coordinates have been deposited in the PDB with accession codes 7PLI (ss-HP92/DbpA complex), 7PMQ (hp-HP92/DbpA complex), and 7PMM (ds-H92/DbpA complex).

SUPPLEMENTAL MATERIAL

Supplemental material is available for this article.

ACKNOWLEDGMENTS

I am indebted to Remco Sprangers for his generous support, fruitful discussions, laboratory space, and spectrometer time. I would like to thank Jens Wöhnert and Konstantin Neißner for the acquisition of the diffraction data of the ss-HP92 RNA/DbpA complex and Olga Rudi for help with protein preparation. The Paul Scherrer Institut, Villigen, Switzerland and the EMBL Hamburg are acknowledged for synchrotron radiation beamtime at beamline P13 at the PETRA III storage ring and at beamline PXI of the SLS. I am grateful to Gregor Madej for help with data acquisition at the Paul Scherrer Institut and would like to thank him as well as Christoph Engel and Ursula Neu for helpful discussions regarding structure refinement. I would also like to thank Johanna Stöfl for laboratory support and Jan Overbeck and Jobst Liebau for critical reading of the manuscript. The Deutsche Forschungs Gemeinschaft is acknowledged for funding (DFG grant no. WU 988/1-1).

Received January 8, 2023; accepted April 29, 2023.

REFERENCES

Afonine PV, Grosse-Kunstleve RW, Echols N, Headd JJ, Moriarty NW, Mustyakimov M, Terwilliger TC, Urzhumtsev A, Zwart PH, Adams PD. 2012. Towards automated crystallographic structure refinement with phenix.refine. *Acta Crystallogr D Biol Crystallogr* **68:** 352–367. doi:10.1107/S0907444912001308

Andreou AZ, Harms U, Klostermeier D. 2019. Single-stranded regions modulate conformational dynamics and ATPase activity of eIF4A to optimize 5′-UTR unwinding. *Nucleic Acids Res* **47:** 5260–5275. doi:10.1093/nar/gkz254

Ballut L, Marchadier B, Baguet A, Tomasetto C, Séraphin B, Le Hir H. 2005. The exon junction core complex is locked onto RNA by inhibition of eIF4AIII ATPase activity. *Nat Struct Mol Biol* **12:** 861–869. doi:10.1038/nsmb990

Bowers HA, Maroney PA, Fairman ME, Kastner B, Lührmann R, Nilsen TW, Jankowsky E. 2006. Discriminatory RNP remodeling by the DEAD-box protein DED1. *RNA* **12:** 903–912. doi:10.1261/rna.2323406

Chen Z, Li Z, Hu X, Xie F, Kuang S, Zhan B, Gao W, Chen X, Gao S, Li Y, et al. 2020. Structural basis of human helicase DDX21 in RNA binding, unwinding, and antiviral signal activation. *Adv Sci* **7:** 2000532. doi:10.1002/advs.202000532

Cianci M, Bourenkov G, Pompidor G, Karpics I, Kallio J, Bento I, Roessle M, Cipriani F, Fiedler S, Schneider TR. 2017. P13, the EMBL macromolecular crystallography beamline at the low-emittance PETRA III ring for high- and low-energy phasing with variable beam focusing. *J Synchrotron Radiat* **24:** 323–332. doi:10.1107/S1600577516016465

Clore GM, Tang C, Iwahara J. 2007. Elucidating transient macromolecular interactions using paramagnetic relaxation enhancement. *Curr Opin Struct Biol* **17:** 603–616. doi:10.1016/j.sbi.2007.08.013

Collins R, Karlberg T, Lehtiö L, Schütz P, van den Berg S, Dahlgren L-G, Hammarström M, Weigelt J, Schüler H. 2009. The DEXD/H-box RNA helicase DDX19 is regulated by an α-helical switch. *J Biol Chem* **284:** 10296–10300. doi:10.1074/jbc.C900018200

Del Campo M, Lambowitz AM. 2009. Structure of the yeast DEAD box protein Mss116p reveals two wedges that crimp RNA. *Mol Cell* **35:** 598–609. doi:10.1016/j.molcel.2009.07.032

Delaglio F, Grzesiek S, Vuister GW, Zhu G, Pfeifer J, Bax A. 1995. NMRPipe: a multidimensional spectral processing system based on UNIX pipes. *J Biomol NMR* **6:** 277–293. doi:10.1007/BF00197809

Diges CM, Uhlenbeck OC. 2001. *Escherichia coli* DbpA is an RNA helicase that requires hairpin 92 of 23S rRNA. *EMBO J* **20:** 5503–5512. doi:10.1093/emboj/20.19.5503

Emsley P, Cowtan K. 2004. *Coot:* model-building tools for molecular graphics. *Acta Crystallogr D Biol Crystallogr* **60:** 2126–2132. doi:10.1107/S0907444904019158

Fairman-Williams ME, Guenther U-P, Jankowsky E. 2010. SF1 and SF2 helicases: family matters. *Curr Opin Struct Biol* **20:** 313–324. doi:10.1016/j.sbi.2010.03.011

Guillerez J, Lopez PJ, Proux F, Launay H, Dreyfus M. 2005. A mutation in T7 RNA polymerase that facilitates promoter clearance. *Proc Natl Acad Sci* **102:** 5958–5963. doi:10.1073/pnas.0407141102

Güntert P, Mumenthaler C, Wüthrich K. 1997. Torsion angle dynamics for NMR structure calculation with the new program DYANA. *J Mol Biol* **273:** 283–298. doi:10.1006/jmbi.1997.1284

Hardin JW, Hu YX, McKay DB. 2010. Structure of the RNA binding domain of a DEAD-box helicase bound to its ribosomal RNA target reveals a novel mode of recognition by an RNA recognition motif. *J Mol Biol* **402:** 412–427. doi:10.1016/j.jmb.2010.07.040

Henn A, Cao W, Licciardello N, Heitkamp SE, Hackney DD, De La Cruz EM. 2010. Pathway of ATP utilization and duplex rRNA unwinding by the DEAD-box helicase, DbpA. *Proc Natl Acad Sci* **107:** 4046–4050. doi:10.1073/pnas.0913081107

Jarmoskaite I, Russell R. 2014. RNA helicase proteins as chaperones and remodelers. *Annu Rev Biochem* **83:** 697–725. doi:10.1146/annurev-biochem-060713-035546

Kabsch W. 2010. Integration, scaling, space-group assignment and post-refinement. *Acta Crystallogr D Biol Crystallogr* **66:** 133–144. doi:10.1107/S0907444909047374

Keller R. 2004. *The computer aided resonance assignment tutorial*. Cantina Verlag, Goldau, Switzerland. ISBN 3-85600-112-3.

Kiianitsa K, Solinger JA, Heyer W-D. 2003. NADH-coupled microplate photometric assay for kinetic studies of ATP-hydrolyzing enzymes with low and high specific activities. *Anal Biochem* **321:** 266–271. doi:10.1016/s0003-2697(03)00461-5

Linder P, Jankowsky E. 2011. From unwinding to clamping—the DEAD box RNA helicase family. *Nat Rev Mol Cell Biol* **12:** 505–516. doi:10.1038/nrm3154

Liu F, Putnam A, Jankowsky E. 2008. ATP hydrolysis is required for DEAD-box protein recycling but not for duplex unwinding. *Proc Natl Acad Sci* **105:** 20209–20214. doi:10.1073/pnas.0811115106

Mallam AL, Del Campo M, Gilman B, Sidote DJ, Lambowitz AM. 2012. Structural basis for RNA-duplex recognition and unwinding by the DEAD-box helicase Mss116p. *Nature* **490:** 121–125. doi:10.1038/nature11402

McCoy AJ, Grosse-Kunstleve RW, Adams PD, Winn MD, Storoni LC, Read RJ. 2007. Phaser crystallographic software. *J Appl Crystallogr* **40:** 658–674. doi:10.1107/S0021889807021206

Montpetit B, Thomsen ND, Helmke KJ, Seeliger MA, Berger JM, Weis K. 2011. A conserved mechanism of DEAD-box ATPase activation by nucleoporins and $InsP_6$ in mRNA export. *Nature* **472:** 238–242. doi:10.1038/nature09862

Mueller M, Wang M, Schulze-Briese C. 2012. Optimal fine ϕ-slicing for single-photon-counting pixel detectors. *Acta Crystallogr D Biol Crystallogr* **68:** 42–56. doi:10.1107/S0907444911049833

Ngo TD, Partin AC, Nam Y. 2019. RNA specificity and autoregulation of DDX17, a modulator of microRNA biogenesis. *Cell Rep* **29:** 4024.e5–4035.e5. doi:10.1016/j.celrep.2019.11.059

Pettersen EF, Goddard TD, Huang CC, Meng EC, Couch GS, Croll TI, Morris JH, Ferrin TE. 2021. UCSF ChimeraX: structure visualization for researchers, educators, and developers. *Protein Sci* **30:** 70–82. doi:10.1002/pro.3943

Putnam AA, Jankowsky E. 2013. DEAD-box helicases as integrators of RNA, nucleotide and protein binding. *Biochim Biophys Acta* **1829:** 884–893. doi:10.1016/j.bbagrm.2013.02.002

Raj S, Bagchi D, Orero JV, Banroques J, Tanner NK, Croquette V. 2019. Mechanistic characterization of the DEAD-box RNA helicase Ded1 from yeast as revealed by a novel technique using single-molecule magnetic tweezers. *Nucleic Acids Res* **47:** 3699–3710. doi:10.1093/nar/gkz057

Ren Y, Schmiege P, Blobel G. 2017. Structural and biochemical analyses of the DEAD-box ATPase Sub2 in association with THO or Yra1. *Elife* **6:** e20070. doi:10.7554/eLife.20070

Richardson JS, Schneider B, Murray LW, Kapral GJ, Immormino RM, Headd JJ, Richardson DC, Ham D, Hershkovits E, Williams LD, et al. 2008. RNA backbone: consensus all-angle conformers and modular string nomenclature (an RNA Ontology Consortium contribution). *RNA* **14:** 465–481. doi:10.1261/rna.657708

Rogers GW, Richter NJ, Merrick WC. 1999. Biochemical and kinetic characterization of the RNA helicase activity of eukaryotic initiation factor 4A. *J Biol Chem* **274:** 12236–12244. doi:10.1074/jbc.274.18.12236

Rossi P, Xia Y, Khanra N, Veglia G, Kalodimos CG. 2016. ^{15}N and ^{13}C-SOFAST-HMQC editing enhances 3D-NOESY sensitivity in highly deuterated, selectively [^{1}H,^{13}C]-labeled proteins. *J Biomol NMR* **66:** 259–271. doi:10.1007/s10858-016-0074-5

Russell R, Jarmoskaite I, Lambowitz AM. 2013. Toward a molecular understanding of RNA remodeling by DEAD-box proteins. *RNA Biol* **10:** 44–55. doi:10.4161/rna.22210

Samatanga B, Klostermeier D. 2014. DEAD-box RNA helicase domains exhibit a continuum between complete functional independence and high thermodynamic coupling in nucleotide and RNA duplex recognition. *Nucleic Acids Res* **42:** 10644–10654. doi:10.1093/nar/gku747

Schanda P, Kupce E, Brutscher B. 2005. SOFAST-HMQC experiments for recording two-dimensional heteronuclear correlation spectra of proteins within a few seconds. *J Biomol NMR* **33:** 199–211. doi:10.1007/s10858-005-4425-x

Sengoku T, Nureki O, Nakamura A, Kobayashi S, Yokoyama S. 2006. Structural basis for RNA unwinding by the DEAD-box protein *Drosophila* Vasa. *Cell* **125:** 287–300. doi:10.1016/j.cell.2006.01.054

Sharpe Elles LM, Sykes MT, Williamson JR, Uhlenbeck OC. 2009. A dominant negative mutant of the *E. coli* RNA helicase DbpA blocks assembly of the 50S ribosomal subunit. *Nucleic Acids Res* **37:** 6503–6514. doi:10.1093/nar/gkp711

Snoussi K, Leroy JL. 2001. Imino proton exchange and base-pair kinetics in RNA duplexes. *Biochemistry* **40:** 8898–8904. doi:10.1021/bi010385d

Sun Y, Atas E, Lindqvist LM, Sonenberg N, Pelletier J, Meller A. 2014. Single-molecule kinetics of the eukaryotic initiation factor 4AI upon RNA unwinding. *Structure* **22:** 941–948. doi:10.1016/j.str.2014.04.014

Theissen B, Karow AR, Köhler J, Gubaev A, Klostermeier D. 2008. Cooperative binding of ATP and RNA induces a closed

conformation in a DEAD box RNA helicase. *Proc Natl Acad Sci* **105:** 548–553. doi:10.1073/pnas.0705488105

Tran EJ, Zhou Y, Corbett AH, Wente SR. 2007. The DEAD-box protein Dbp5 controls mRNA export by triggering specific RNA:protein remodeling events. *Mol Cell* **28:** 850–859. doi:10.1016/j.molcel.2007.09.019

Tsu CA, Uhlenbeck OC. 1998. Kinetic analysis of the RNA-dependent adenosinetriphosphatase activity of DbpA, an *Escherichia coli* DEAD protein specific for 23S ribosomal RNA. *Biochemistry* **37:** 16989–16996. doi:10.1021/bi981837y

Wang S, Hu Y, Overgaard MT, Karginov FV, Uhlenbeck OC, McKay DB. 2006. The domain of the *Bacillus subtilis* DEAD-box helicase YxiN that is responsible for specific binding of 23S rRNA has an RNA recognition motif fold. *RNA* **12:** 959–967. doi:10.1261/rna.5906

Wong EV, Cao W, Vörös J, Merchant M, Modis Y, Hackney DD, Montpetit B, De La Cruz EM. 2016. P_i release limits the intrinsic and RNA-stimulated ATPase cycles of DEAD-box protein 5 (Dbp5). *J Mol Biol* **428:** 492–508. doi:10.1016/j.jmb.2015.12.018

Wurm JP. 2020. Assignment of the Ile, Leu, Val, Met and Ala methyl group resonances of the DEAD-box RNA helicase DbpA from *E. coli*. *Biomol NMR Assign* **15:** 121–128. doi:10.1007/s12104-020-09994-z

Wurm JP, Glowacz K-A, Sprangers R. 2021. Structural basis for the activation of the DEAD-box RNA helicase DbpA by the nascent ribosome. *Proc Natl Acad Sci* **118:** e2105961118. doi:10.1073/pnas.2105961118

Xiol J, Spinelli P, Laussmann MA, Homolka D, Yang Z, Cora E, Couté Y, Conn S, Kadlec J, Sachidanandam R, et al. 2014. RNA clamping by Vasa assembles a piRNA amplifier complex on transposon transcripts. *Cell* **157:** 1698–1711. doi:10.1016/j.cell.2014.05.018

Yang Q, Del Campo M, Lambowitz AM, Jankowsky E. 2007. DEAD-box proteins unwind duplexes by local strand separation. *Mol Cell* **28:** 253–263. doi:10.1016/j.molcel.2007.08.016